Multiple Sclerosis Lesions Affect Intrinsic Functional Connectivity of the Spinal Cord

Supplementary Material

Supplementary Methods: Preprocessing. The preprocessing pipeline was the same for all subjects. The core script was written in MATLAB using AFNI (Cox, 1996) functions, and has been previously described in detail (Barry *et al.*, 2016). In brief, the general procedure for each slice (12 slices per subject) involved:

1) Manual segmentation of gray matter (GM), white matter (WM), and cerebrospinal fluid (CSF) in the anatomical image using FSLView (Smith *et al.*, 2004) as well as creation of a "not-spine" mask on the functional data which included all voxels outside of the spinal canal. While automatic GM segmentation methods have improved (Asman *et al.*, 2014; De Leener *et al.*, 2016; Prados *et al.*, 2017), including robust GM segmentation in the presence of multiple sclerosis lesions in 3T-acquired data (Prados *et al.*, 2016; Xu *et al.*, 2016), further development of these techniques is necessary to reach the accuracy of a human rater for patients with large lesions similar in appearance to GM on T2*w images as well as in 7T-acquired data. Therefore, we opted for manual segmentation of all subjects in this analysis.
2) Initial denoising by performing principal component analysis (PCA) of voxels within the not-spine mask and then regression of the top components from all voxels. The number of eigenvectors (components) selected reflected up to 80% of the slice-wise cumulative variance or until the difference between two successive eigenvalues was less than 5%.
3) Motion correction procedure. Involved automatic determination of a reference time point, creation of a 2D Gaussian mask around the spinal canal, and rigid-body motion correction allowing for within-plane translation.
4) RETROICOR ("retrospective image correction") (Glover *et al.*, 2000) using the cardiac and respiratory traces to further reduce periodic fluctuations resulting from non-neural physiologic processes.
5) Coregistration procedure for aligning functional images to the anatomical data. Allowed for in-plane translation and scaling, including coarse and fine pass registration steps, and finally resampling of the functional data to the high-resolution space (0.31×0.31 mm^2) using sinc interpolation.
6) CSF denoising. PCA of voxels within the CSF and then regression of the top components from all spinal cord voxel time series (the number of eigenvectors selected reflected up to 50% of the slice-wise cumulative variance or until the difference between two successive eigenvalues was less than 5%).
7) WM denoising. PCA of voxels within the WM and then regression of the first principal component (typically representing 10-40% of the remaining variance) from all spinal cord voxel time series. TSNR in GM was calculated after this processing step.
8) Bandpass filtering of voxelwise time series using a frequency range of 0.01 – 0.13 Hz.

All data were visually inspected at each stage in the processing pipeline. We observed that the automatic coregistration procedure did not perform optimally in approximately 4% of all slices (corresponding to regions of significant signal drop-out and/or geometric distortions). In such cases, alignment of the functional to anatomical data was manually adjusted using a series of rigid body translations. In an effort to preserve the spatial specificity of signals and avoid partial volume effects both within (e.g. among GM horns) and across tissue types, we did not perform spatial smoothing. It should be noted however that some smoothing is inherently introduced when resampling the functional voxels in anatomical image space during step #5 above. The bandpass filtered data from step #8 served as the final preprocessed time series data from which region of interest (ROI)-based correlation and power spectra analyses were conducted. Power spectra were also calculated at each preprocessing step and are plotted in Supplementary Fig. 1.

Supplementary Discussion: Increased ventral network connectivity in females. One unexpected finding from the analysis of our control data was a significant increase in V-V connectivity in females compared to males (Fig. 2D). This is in accord with several reports of gender differences in brain functional connectivity including: increased connectivity in females among default mode regions (Biswal *et al.*, 2010) as well as basal ganglia structures (Allen *et al.*, 2011), more symmetric network organization in females (Liu *et al.*, 2009), stronger connectivity in females involving left amygdala with a number of regions (Kogler *et al.*, 2016), and widespread increases in functional connectivity density (a voxelwise measure which is maximized in highly connected hub regions) across both cortical and subcortical areas in females, with no increases observed in males (Tomasi and Volkow, 2012) (for a review of gender differences in brain connectivity, including a larger body of work looking at differences in anatomical and structural connectivity measures, see Gong et al.) (Gong *et al.*, 2011). Additionally, recent work looking at structural connectivity via diffusion weighted MRI found that the female connectome was generally "better" connected based on a number of graph theoretic measures (e.g. more edges compared to males) (Szalkai *et al.*, 2015). It is plausible that our finding of increased connectivity between ventral horn GM in females is related to more general mechanisms subserving gender differences in organization of the central nervous system, such as via differences in glucose metabolism (Baxter *et al.*, 1987) or sex hormone levels. Given the corticospinal projections innervating ventral horn GM, we may expect that the intrinsic functional organization of spinal cord V-V networks would relate to the brain motor networks. Despite the more general findings of increased connectivity in females highlighted above, there are reports of increased connectivity in males specifically among sensorimotor regions (Filippi *et al.*, 2013) as well as increased connectivity between distinct motor networks compared to females (Allen *et al.*, 2011). In order to understand this potential discrepancy in a gender effect on brain and spinal cord motor networks, more fundamental work is necessary in describing the coherence of brain and spinal cord resting-state networks.

It is important to note that female subjects also demonstrated higher median TSNR values (additionally, gender and TSNR were correlated in patients at $r = 0.64$, Supplementary Fig. 3). The increase in TSNR in

females, indicating an improvement in data quality, could for instance be related to more effective shimming and/or reduced distortions of the magnetic field due to generally smaller body masses in females compared to males. For example, shifts in the B0 field induced by respiratory motion are likely to be greater on average in males. In light of these associations we included both gender and TSNR in our linear models assessing group-level and lesion-specific effects on connectivity. However, to address the possibility that increased V-V connectivity in females was due to differences in TSNR or body mass, we fit a linear model similar to those presented in Supplementary Fig. 4 to predict mean V-V connectivity in our control subject data, with the following predictor variables: age, gender, median TSNR in GM, and subject weight. These results indicated that gender was the only variable significantly associated with V-V connectivity (estimate = 1.73, $p = 0.005$), suggesting that the increase in females was not an artifact of our imaging protocol. Nevertheless, we hold out the possibility for a confounding factor driving this observation and further work is needed to confirm gender differences in intrinsic spinal cord connectivity.

Supplementary Discussion: Limitations. The following section provides more detailed discussion and some additional references concerning the limitations outlined in the main manuscript.

1) Our lesion rating strategy only provided a coarse identification of lesion location, rather than tract-specific identification. For instance, the inclusion of multiple lateral column lesions into a single explanatory variable neglects the heterogeneous spatial distribution and extent of such lesions and therefore their potentially heterogeneous functional consequences (e.g. see Fig. 2, discrepancy between left lateral column lesions in MS03 and MS05). A focal lesion in the lateral corticospinal tract innervating cervical ventral GM, for example, may have a specific effect on cervical V-V connectivity. On the other hand, a nearby lesion involving only sacral corticospinal axons may have no impact on the function of cervical GM. Furthermore, lesions in anterior portions of the lateral column involving spinothalamic tracts may have more specific effects on functional activity or organization in regions to which they project, such as thalamus and sensorimotor cortices. Future work with a larger sample of homogenous lesions, as well as controlled animal models, is needed to clarify the effects of tract-specific damage on functional connectivity in the spinal cord and brain.

2) Our functional imaging approach and GM ROI definitions still only a provide a coarse measurement of functional connectivity among populations of spinal cord neurons. Anatomical and electrophysiological evidence suggests that there are subregions of the GM horns which have distinct efferent and afferent projections (Purves *et al.*, 2012; Kandel *et al.*, 2013). It is possible that these regions demonstrate distinct functional networks which may be more or less affected by lesions within particular WM tracts. Increasing the spatial resolution of spinal cord fMRI may thus provide new insights into BOLD activity within GM subregions. Further is necessary however in determining the specificity of neuronal activation at this scale, as well as the BOLD point spread function in the spinal cord at different field strengths (Summers and Brooks, 2014).

3) There is growing appreciation for the prevalence and impact of cortical GM lesions in multiple sclerosis (Calabrese *et al.*, 2013), with a recent 7T study showed that both cortical and WM lesion volumes were positively correlated with EDSS scores and cognitive impairment (Harrison *et al.*, 2015). We were unable to distinguish GM lesions with our T2*-weighted anatomical sequence and thus could not assess the potential presence or effects of cervical cord GM lesions. It is possible that BOLD signal measured in patient GM regions may thus be confounded by non-neural effects from lesioned tissue. Future work looking at fMRI of the spinal cord in multiple sclerosis may investigate GM lesions using complimentary anatomical sequences such as magnetization-prepared rapid acquisition of gradient echoes (MPRAGE) or magnetization- prepared fluid-attenuated inversion recovery (MPFLAIR) (Nelson *et al.*, 2008; De Graaf *et al.*, 2012). Furthermore, implementation of these techniques at ultra-high field (7T), given the increased signal to noise ratio and higher achievable resolutions, might be necessary to detect lesions at the small scale of spinal cord GM (Sinnecker *et al.*, 2012; Harrison *et al.*, 2015).

4) Another limitation to note is that we did not measure lesions in the brain or cord outside the imaging volume that spanned just 4.8 centimeters along the cervical cord. We must consider the possibility that abnormal spinal cord activity in multiple sclerosis could be influenced by long-distance modulation from projection areas in brain and brainstem, due to structural damage in connecting fiber tracts and/or functional reorganization of those circuits. It may be that downstream and/or upstream effects of more distant structural damage influence the connectivity profiles of GM in the cervical cord in multiple sclerosis. Future studies of functional connectivity in the cord should at the very least consider acquisition of anatomical images of the brain to assess lesion burden and location in cortical and subcortical WM and brainstem. Whole brain and GM atrophy as well as WM integrity, as measured by diffusion-weighted imaging, may also be considered in relation to cord function. The RF-coil used is this study was specifically designed for cervical cord imaging and thus did not allow for whole brain coverage. In addition to structural imaging, improvements in coil hardware and coverage as well as accelerated fMRI acquisition techniques may provide opportunities to assess BOLD signal fluctuations in larger segments of the cord and brain simultaneously at adequate resolutions. Such studies are likely to offer a more complete view of brain-spinal cord interactions, including the intrinsic functional organization of these networks at rest in health and disease.

Supplementary Figure 1. Power Spectral Density through Preprocessing Steps in Controls. Power spectra for all cord voxels (i.e. included GM and WM) were estimated using a fast Fourier transform and the subject mean spectra (n=56) were averaged across the group. No bandpass filtering was applied. Mean power spectra were calculated after each step of preprocessing, described in detail in the Methods section. In general, each step explained some additional variance and the overall power decreased accordingly. As seen in the final bandpassed data presented in Fig. 2E, the peak at 0.075Hz appeared after CSF denoising, and most prominently after the final step of WM denoising. NSnoise = "not-spine" mask denoising; MC = motion correction; Ricor = RETROICOR correction; Warp = coregistration/interpolation to anatomical space; CSFnoise = CSF denoising; WMnoise = WM denoising.

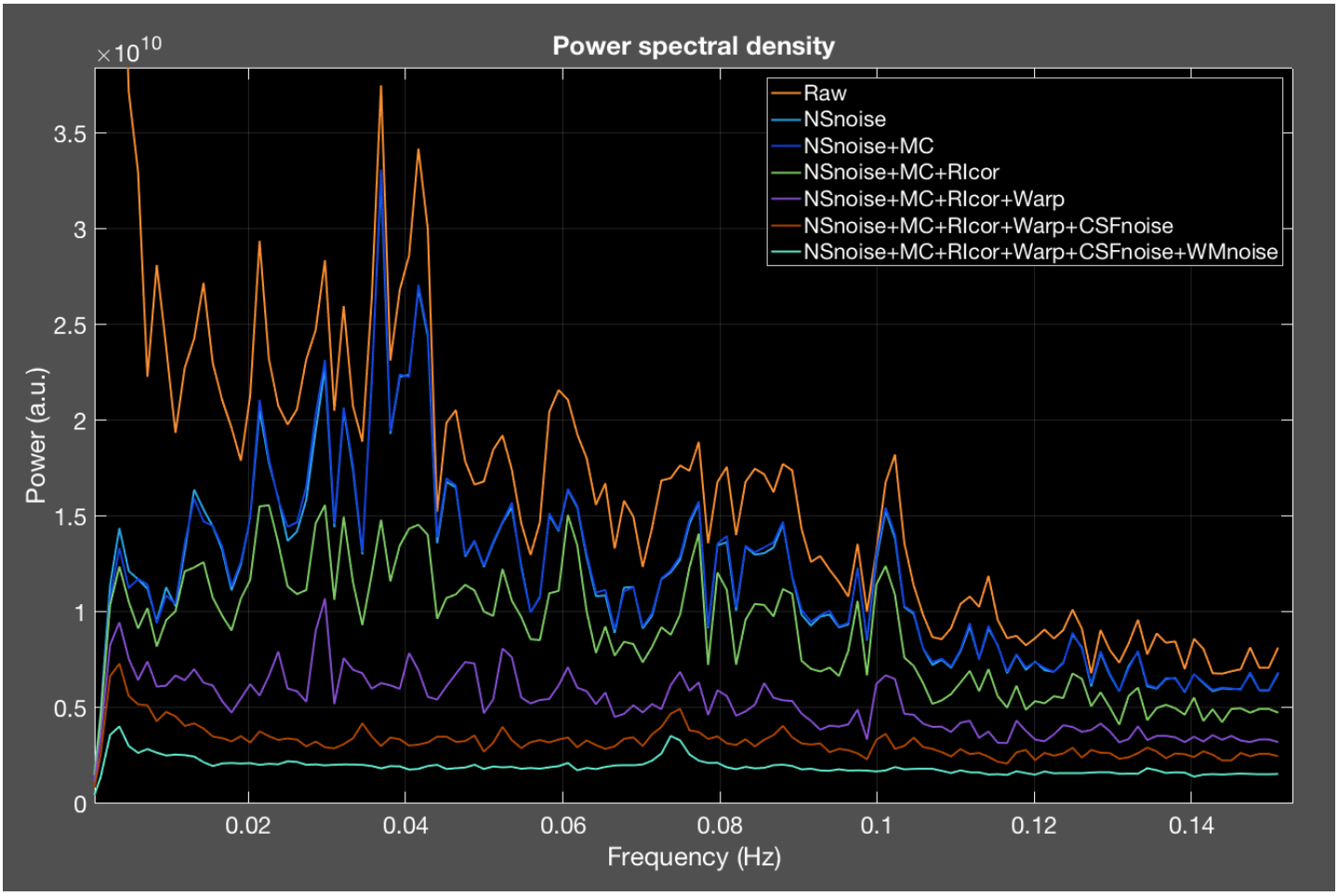

Supplementary Figure 2. Mean Connectivity by Bandpass Frequency Range in Controls. The mean z-score across 12 slices for each ROI pair was calculated in control subjects (n=56). Boxplots of mean z-scores for each ROI pairing are presented after bandpass filtering over different frequency windows. The 0.01-0.13Hz window was considered the full range, as employed in preprocessing, and those data are identical to the control plots from Fig. 2F. The full range was broken into three sub-ranges: slow (0.01-0.065Hz), medium (0.065-0.085Hz), and fast (0.085-0.13Hz). The medium range was intended to capture the frequencies contributing to the spike in power at approximately 0.075Hz, as seen in Fig. 2E and Supplementary Fig. 1 (after CSF/WM denoising steps). Two-tailed Wilcoxon rank-sum tests were performed between the sub-range data for each ROI pair, with asterisks indicating where significant differences were detected, $*P < 0.01$, $**P < 0.001$, $***P < 0.0001$. Increased z-scores were observed for V-V, D-D, LV-LD, and RV-RD over the medium range compared to the slow and fast ranges. Furthermore, there were no significant differences in z-scores when comparing the full range data to the medium sub-range data. Taken together, these findings suggest that intrinsic fluctuations in BOLD signal at frequencies from 0.065-0.085Hz strongly contribute to functional connectivity in the cervical cord. It should be noted, however, that connectivity values in the slow and fast sub-ranges were still more similar within the ROI pair comparisons (e.g. slow/fast V-V z-scores were higher than slow/fast D-D z-scores), suggesting that these frequency ranges do carry useful information in regards to spinal cord functional connectivity.

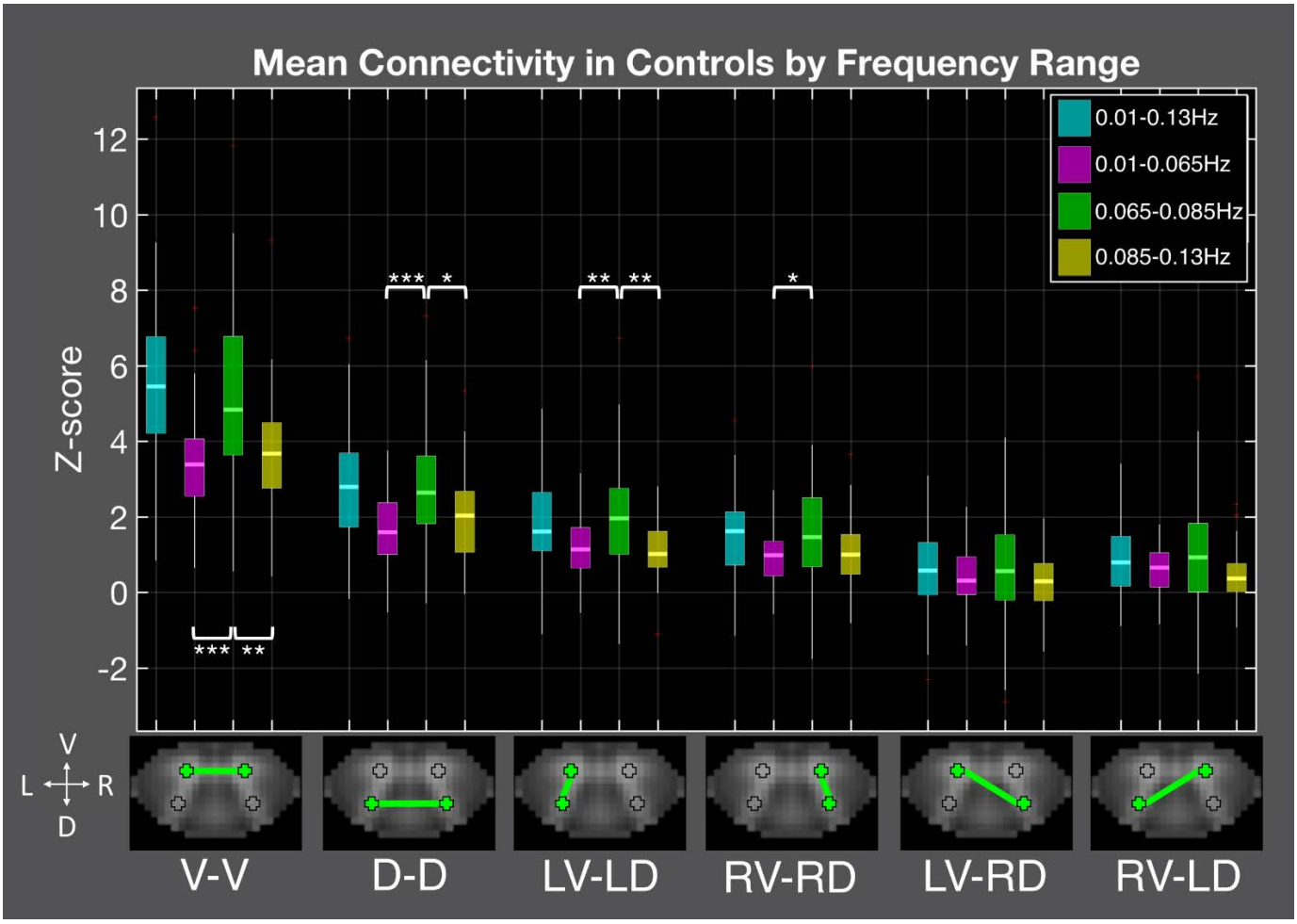
Mean Connectivity in Controls by Frequency Range
0.01-0.13Hz
0.01-0.065Hz
0.065-0.085Hz
0.085-0.13Hz
Z-score
12
10
8
6
4
2
0
-2
***
*
**
**
*
***
**
V
L
R
D
V-V
D-D
LV-LD
RV-RD
LV-RD
RV-LD

Supplementary Figure 3. Patient Variable Correlations (Pearson's *r* values). A cross-correlation matrix is provided depicting the correlation strength (Pearson's *r*) between a number of variables acquired in the study. Correlations were computed independently and using only values from the patient sample (n=22). The matrix is symmetric across the diagonal; thus, those values along with correlation strength of a variable with itself (along diagonal) were excluded. Red and blue color scale indicates positive and negative *r* values, respectively, and the opacity of the filled-in color is proportional to the *r* value. Dark boxes around particular cells indicate a *p* value < 0.05. Variables were categorized into three groups for readability (Demographics, Connectivity, and Lesion Presence). Connectivity values (V-V, D-D, LV-LD, RV-RD, LV-RD, and RV-LD) were subject's average ROI pair z-scores over 12 slices. Lesion values were included as a percentage of total rated slices containing the specified lesion (e.g. rather than the total count, since two patients had slices which were excluded from the lesion ratings, see Fig. 3 - MS03 and MS18), where LesionCount and LCount = total count of columns/slices rated as containing a lesion in each subject; TSNR = average TSNR across 12 slices (from slicewise median TSNR in GM); Below = percentage of slices below a descending tract lesion in each subject; Above = percentage of slices above an ascending tract lesion. Demographic measures of clinical severity were significantly correlated, such as EDSS and disease duration (r = 0.42) and EDSS and 25ftWalk (r = 0.79). Lesion count was positively correlated with EDSS (r = 0.61) and disease duration (r = 0.46), as well as with RV-RD connectivity (r = 0.47) and TSNR (r = 0.45). Higher number of individual column lesions were also generally associated with increased disability measures. For instance, dorsal column lesion presence was positively correlated with both multiple sclerosis duration and EDSS, while left lateral lesion presence was correlated with increased EDSS and 25ft-walk times. The mean connectivity strength for V-V and D-D were positively correlated with each other but did not reach significance in relation to other variables. While not the focus of this work, interesting relationships were observed in which the presence of left lateral, right lateral, and dorsal column lesions were significantly correlated amongst each other, suggesting that the appearance of a lesion in one column is predictive of additional lesions in other columns.

		Demographics							Connectivity						Lesion Presence					
		Age	*Gender*	*EDSS*	*MSDur*	*25ftWalk*	*LCount*	*TSNR*	*V-V*	*D-D*	*LV-LD*	*RV-RD*	*LV-RD*	*RV-LD*	*L lesion*	*R lesion*	*D lesion*	*V lesion*	*Below*	*Above*
Demographics	***Age***																			
	Gender	-0.10																		
	EDSS	0.48	0.14																	
	MSDuration	0.17	0.29	0.42																
	25ftWalk	0.34	0.28	0.79	0.27															
	LesionCount	0.21	0.32	0.61	0.46	0.37														
	TSNR	-0.09	0.64	0.29	0.24	0.37	0.45													
Connectivity	***V-V***	-0.33	-0.06	-0.12	0.06	0.07	-0.09	-0.41												
	D-D	-0.27	0.15	0.31	0.31	0.30	0.20	0.02	0.64											
	LV-LD	0.19	-0.22	0.11	-0.32	-0.05	-0.13	-0.19	-0.07	-0.05										
	RV-RD	0.14	0.11	0.33	0.18	0.07	0.47	0.15	-0.08	0.15	0.36									
	LV-RD	0.19	-0.02	0.36	0.24	0.02	0.35	-0.12	-0.03	0.32	0.11	0.75								
	RV-LD	0.08	-0.06	0.20	-0.08	0.03	0.01	0.17	-0.03	0.22	0.69	0.41	0.17							
Lesion Presence	***L lesions***	0.15	0.25	0.61	0.15	0.47	0.71	0.39	-0.15	0.22	-0.03	0.19	0.29	-0.02						
	R lesions	-0.01	0.48	0.41	0.34	0.27	0.76	0.46	0.01	0.11	-0.03	0.38	0.15	-0.04	0.43					
	D lesions	0.35	0.20	0.50	0.45	0.26	0.80	0.06	0.14	0.33	-0.07	0.45	0.44	0.10	0.51	0.42				
	V lesions	0.00	-0.14	0.05	0.35	0.06	0.27	0.29	-0.19	-0.09	-0.22	0.19	-0.05	0.00	-0.22	0.07	0.09			
	Below	0.09	0.23	0.39	0.26	0.33	0.68	0.41	-0.33	-0.15	-0.15	0.18	0.11	-0.35	0.63	0.53	0.29	0.35		
	Above	0.25	0.14	0.51	0.04	0.24	0.65	0.28	-0.39	-0.19	0.15	0.37	0.31	0.20	0.51	0.50	0.50	0.10	0.46	
		Age	*Gender*	*EDSS*	*MSDur*	*25ftWalk*	*LCount*	*TSNR*	*V-V*	*D-D*	*LV-LD*	*RV-RD*	*LV-RD*	*RV-LD*	*L lesion*	*R lesion*	*D lesion*	*V lesion*	*Below*	*Above*

Supplementary Figure 4. Linear Models to Assess Group Effects. Results of multiple linear regression models performed separately for each ROI pairing are presented, looking for an effect of group while controlling for other variables. The dependent variable in each model was subject average ROI pair z-score over 12 slices. Four predictor variables were included: group (Control/Patient), age, gender (Male/Female), and median temporal signal to noise ratio in GM. The main effect of each variable is depicted along with confidence intervals. There were no significant main effects of group for any of the six ROI pairing z-scores. Significant effects of gender and TSNR were found in association with V-V z-scores.

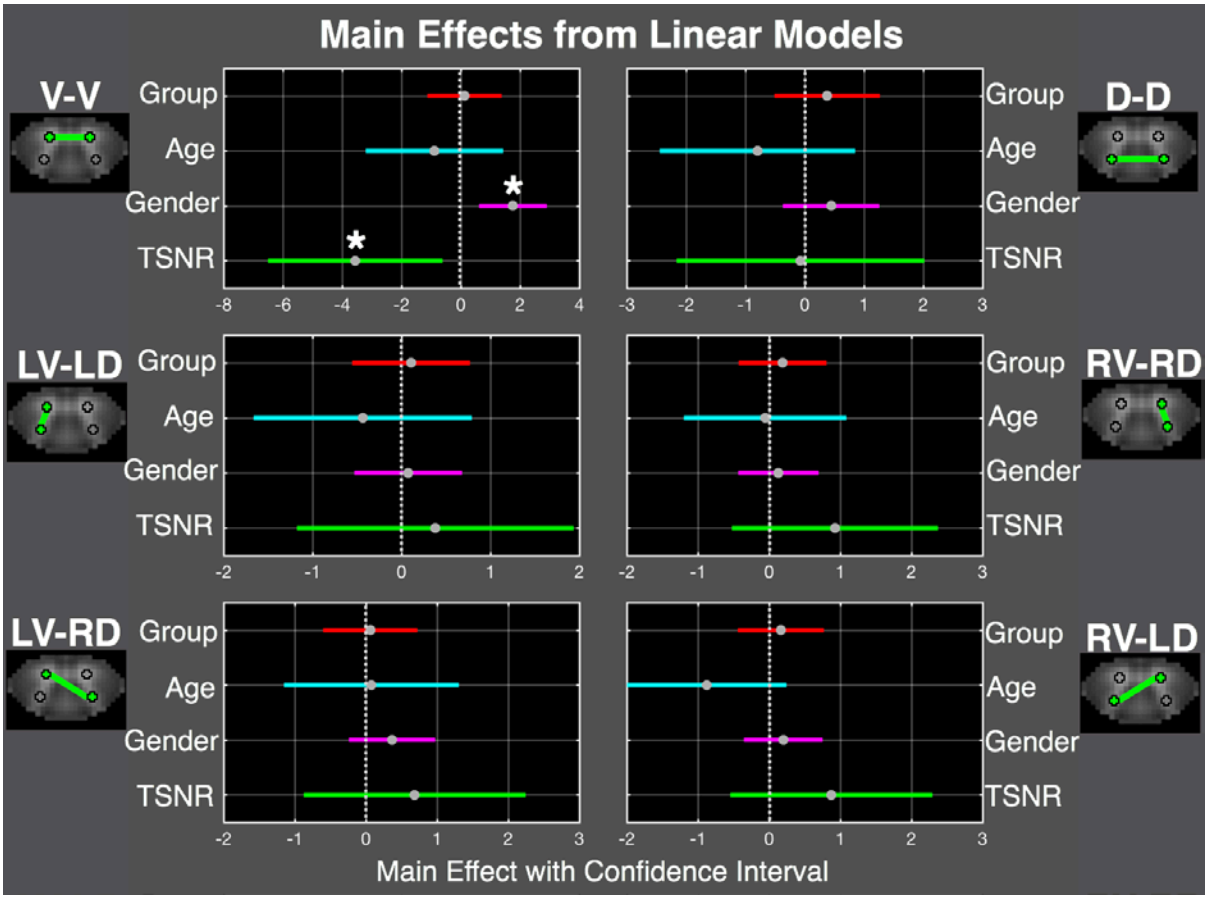

Supplementary Figure 5. Linear Models to Assess Effects of Patient Variables. Results of multiple linear regression models performed separately for each ROI pairing are presented (the subpanels 1-6 correspond to V-V, D-D, LV-LD, RV-RD, LV-RD, and RV-LD respectively) looking for an effect of the variable of interest (always yellow) while controlling for Age, Gender and TSNR, which mirrors the covariates we controlled for in Figures 4, 5, and Supplementary Figure 4. These models were conducted within the patient group only. The dependent variable in each model was subject average ROI pair z-score over 12 slices, thus there were 22 observations for each ROI pairing. Four predictor variables were included: age (range = 22-61 years), gender (Male = 0, Female = 1), and median temporal signal to noise ratio in GM (TSNR, range = 15.4-49.9), and the clinical variable of interest, as indicated in the title of each subset. The main effect of each variable is depicted along with 95% confidence intervals. Variables in which the confidence interval does not cross zero (red line) indicate a significant main effect of the variable. Asterisks indicate the variables showing a significant effect at $P<0.05$. There were modest significant associations of EDSS and 25 Foot Walk times with D-D connectivity, as well an association of 25 Foot Walk times with V-V connectivity (all positive effects). These findings indicate increasing disability is related to increased bilateral connectivity, and it is possible this reflects a compensatory mechanism of increased communication among bilateral spinal cord networks. However, more work with a larger sample size is required to confirm this observation.

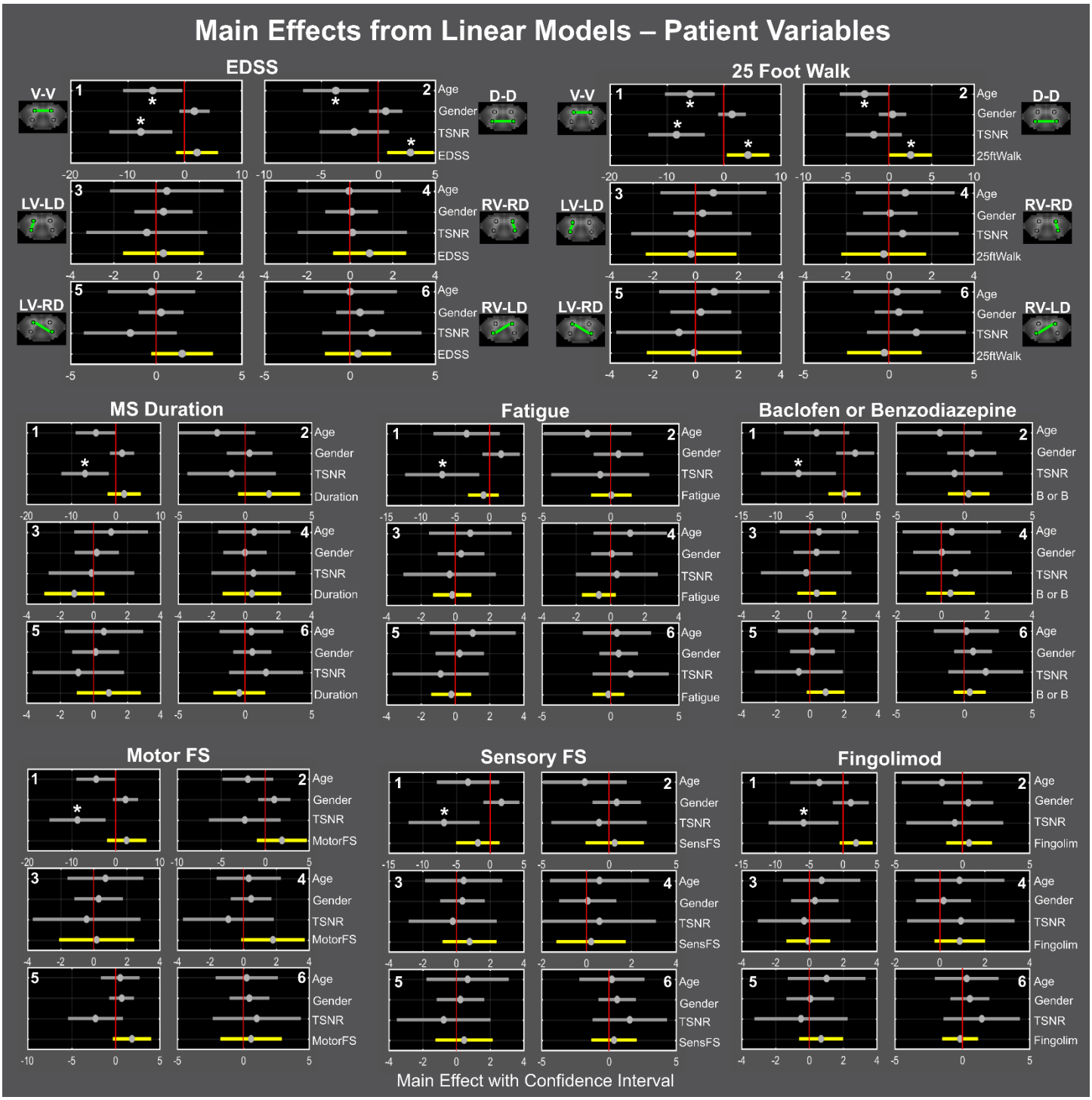
Main Effects from Linear Models – Patient Variables
EDSS
25 Foot Walk
MS Duration
Fatigue
Baclofen or Benzodiazepine
Motor FS
Sensory FS
Fingolimod
V-V
D-D
LV-LD
RV-RD
LV-RD
RV-LD
Age
Gender
TSNR
EDSS
25ftWalk
Duration
Fatigue
B or B
MotorFS
SensFS
Fingolim
Main Effect with Confidence Interval

Supplementary Table 1. Clinical demographics/symptoms in individual patients

Subject	Age	Gender	EDSS	MSDuration	25ftWalk	Handedness	Medication	Fatigue	Motor FS (Functional Systems) score	Sensory FS score	Bladder FS score	Clinical comments	Baclofen (1) or benzodiazepines (2)?
MS01	55	Male	5	5	8	R	Mycophenolate	1	2	0	0	Legs get wobbly after walking 1-2 blocks	0
MS02	35	Female	0	1	4.1	R	IFN beta 1a	0	0	0	0		0
MS03	49	Male	3.5	14	4.6	R	IFN beta 1a	1	1	3	2	Loss of vibration and joint position is the main issue	
MS04	32	Male	0	1	4.1	R	IFN beta 1a	0	0	0	0		0
MS05	49	Female	3	2	9.8	R	Natalizumab	1	0	2	2	Decreased proprioception, bladder urgency	1
MS06	40	Female	6	8	13	R	Fingolimod	0	4	0	0	Weakness in all extremities	1
MS07	31	Female	0	6	3.8	R	Fingolimod	0	0	0	0		0
MS08	48	Female	2	7	5.4	R	Fingolimod	0	0	0	0	Visual acuity 20/30	0
MS09	48	Male	0	8	4	L	Fingolimod	0	0	0	0		0
MS10	42	Female	6	19	6.8	R	Fingolimod	1	3	3	2	Cane use due to ataxia and LE weakness	1
MS11	38	Male	0	1	4.5	R	Fingolimod	0	0	0	0		0
MS12	31	Female	1.5	13	5.8	R	Fingolimod	1	0	0	0		0
MS13	43	Female	1.5	23	4.1	L	Fingolimod	1	0	0	0	Difficulty tandem gait	1
MS14	50	Male	2	4	6.3	R	Fingolimod	1	0	2	0	Loss of vibration sense in toes	2
MS15	61	Male	3	9	5.8	R	Fingolimod	1	0	0	0	Trigeminal neuralgia	1
MS16	41	Female	2	18	6.5	R	Fingolimod	1	0	0	0	Cognitive issues	0
MS17	41	Male	3.5	26	8.2	R	Fingolimod	0	2	0	0	Internuclear ophthalmoplegia	0
MS18	48	Female	6	21	13	R	Fingolimod	0	0	0	0	Use of cane for gait ataxia	0
MS19	44	Female	2.5	12	5	R	Fingolimod	0	0	0	2	Bladder urgency and gait ataxia	0
MS20	22	Male	0	5	4.2	R	Fingolimod	0	0	0	0		0
MS21	38	Female	0	12	5	R	Fingolimod	0	0	0	0		0
MS22	30	Male	2.5	3	4.1	R	Fingolimod	1	0	0	0		1

Supplementary Table 2. Local Effects of Lesions on Functional Connectivity – Full Statistical Results

	Name	Estimate	SE	tStat	DF	*P*-value	Lower	Upper
V-V	**Intercept**	5.55	1.00	5.56	922	0.000*	3.59	7.51
	Group	0.25	0.67	0.37	922	0.709	-1.06	1.56
	Age	-0.01	0.03	-0.35	922	0.725	-0.06	0.04
	Gender	1.11	0.50	2.20	922	0.028*	0.12	2.10
	TSNR	-0.01	0.02	-0.51	922	0.611	-0.04	0.02
	L lesion	0.08	0.44	0.18	922	0.857	-0.79	0.95
	R lesion	-0.30	0.48	-0.63	922	0.531	-1.25	0.65
	D lesion	-0.47	0.48	-0.98	922	0.329	-1.41	0.47
	V lesion	-1.17	0.58	-2.03	922	0.043*	-2.30	-0.04
D-D	**Intercept**	1.18	0.80	1.49	922	0.137	-0.38	2.75
	Group	-0.78	0.50	-1.56	922	0.118	-1.77	0.20
	Age	-0.01	0.02	-0.69	922	0.490	-0.05	0.02
	Gender	-0.08	0.37	-0.22	922	0.826	-0.81	0.64
	TSNR	0.06	0.01	4.07	922	0.000*	0.03	0.09
	L lesion	0.88	0.44	2.03	922	0.043*	0.03	1.74
	R lesion	0.66	0.48	1.37	922	0.171	-0.28	1.60
	D lesion	0.15	0.47	0.32	922	0.746	-0.76	1.07
	V lesion	-0.37	0.57	-0.65	922	0.516	-1.49	0.75
LV-LD	**Intercept**	1.73	0.49	3.56	922	0.000*	0.78	2.69
	Group	0.05	0.27	0.17	922	0.863	-0.47	0.57
	Age	-0.01	0.01	-0.95	922	0.345	-0.03	0.01
	Gender	-0.09	0.19	-0.46	922	0.646	-0.46	0.28
	TSNR	0.01	0.01	1.08	922	0.282	-0.01	0.03
	L lesion	0.38	0.36	1.06	922	0.289	-0.32	1.08
	R lesion	0.08	0.39	0.20	922	0.841	-0.70	0.85
	D lesion	-0.19	0.37	-0.52	922	0.604	-0.91	0.53
	V lesion	-0.48	0.47	-1.02	922	0.310	-1.40	0.45
RV-RD	**Intercept**	0.93	0.49	1.91	922	0.056	-0.02	1.89
	Group	-0.10	0.26	-0.38	922	0.702	-0.62	0.42
	Age	0.00	0.01	-0.33	922	0.745	-0.02	0.01

	Gender	-0.16	0.19	-0.88	922	0.382	-0.53	0.20
	TSNR	0.02	0.01	1.99	922	0.047*	0.00	0.05
	L lesion	-0.40	0.36	-1.12	922	0.262	-1.10	0.30
	R lesion	0.87	0.39	2.20	922	0.028*	0.09	1.64
	D lesion	0.71	0.37	1.93	922	0.053	-0.01	1.43
	V lesion	-0.02	0.47	-0.05	922	0.961	-0.95	0.90
LV-RD	**Intercept**	0.34	0.50	0.69	922	0.489	-0.63	1.31
	Group	-0.34	0.27	-1.24	922	0.215	-0.86	0.19
	Age	0.00	0.01	-0.27	922	0.790	-0.02	0.02
	Gender	-0.40	0.19	-2.07	922	0.039*	-0.77	-0.02
	TSNR	0.01	0.01	1.27	922	0.204	-0.01	0.04
	L lesion	0.46	0.36	1.28	922	0.200	-0.25	1.18
	R lesion	0.07	0.40	0.17	922	0.863	-0.72	0.86
	D lesion	0.78	0.37	2.10	922	0.036*	0.05	1.52
	V lesion	-0.03	0.48	-0.06	922	0.954	-0.97	0.91
RV-LD	**Intercept**	0.80	0.49	1.64	922	0.100	-0.16	1.76
	Group	-0.33	0.27	-1.22	922	0.221	-0.85	0.20
	Age	-0.02	0.01	-2.29	922	0.022*	-0.04	0.00
	Gender	-0.16	0.19	-0.87	922	0.383	-0.54	0.21
	TSNR	0.02	0.01	1.78	922	0.075*	0.00	0.04
	L lesion	0.19	0.36	0.53	922	0.595	-0.51	0.89
	R lesion	-0.02	0.40	-0.05	922	0.964	-0.80	0.76
	D lesion	0.54	0.37	1.46	922	0.144	-0.18	1.26
	V lesion	-0.55	0.47	-1.17	922	0.242	-1.48	0.37

Supplementary Table 3. Distal Effects of Lesions on Functional Connectivity – Full Statistical Results

	Name	Estimate	SE	tStat	DF	*P*-value	Lower	Upper
V-V	**Intercept**	5.42	0.99	5.50	929.00	0.000*	3.48	7.35
	Group	0.56	0.74	0.75	929.00	0.452	-0.89	2.00
	Age	-0.01	0.03	-0.37	929.00	0.714	-0.06	0.04
	Gender	1.09	0.49	2.22	929.00	0.027*	0.13	2.06
	TSNR	0.00	0.02	-0.23	929.00	0.815	-0.03	0.03
	Below	-0.69	0.46	-1.51	929.00	0.131	-1.59	0.21
	Above	-0.32	0.43	-0.74	929.00	0.457	-1.16	0.52
D-D	**Intercept**	0.98	0.79	1.25	929.00	0.212	-0.56	2.52
	Group	-0.03	0.58	-0.05	929.00	0.959	-1.17	1.11
	Age	-0.01	0.02	-0.61	929.00	0.543	-0.05	0.02
	Gender	0.00	0.36	0.00	929.00	0.999	-0.70	0.71
	TSNR	0.06	0.01	4.26	929.00	0.000*	0.03	0.09
	Below	-0.34	0.44	-0.78	929.00	0.435	-1.21	0.52
	Above	-0.16	0.42	-0.38	929.00	0.707	-0.98	0.66
LV-LD	**Intercept**	1.71	0.49	3.50	929.00	0.000*	0.75	2.66
	Group	0.07	0.34	0.20	929.00	0.841	-0.60	0.74
	Age	-0.01	0.01	-1.05	929.00	0.292	-0.03	0.01
	Gender	-0.10	0.18	-0.55	929.00	0.581	-0.46	0.26
	TSNR	0.01	0.01	1.23	929.00	0.218	-0.01	0.04
	Below	0.19	0.33	0.56	929.00	0.577	-0.47	0.84
	Above	-0.11	0.33	-0.33	929.00	0.739	-0.76	0.54
RV-RD	**Intercept**	0.88	0.49	1.79	929.00	0.073	-0.08	1.84
	Group	-0.09	0.34	-0.26	929.00	0.799	-0.76	0.59
	Age	0.00	0.01	-0.29	929.00	0.775	-0.02	0.01
	Gender	-0.12	0.19	-0.65	929.00	0.518	-0.49	0.24
	TSNR	0.02	0.01	2.03	929.00	0.043*	0.00	0.05
	Below	0.13	0.33	0.38	929.00	0.707	-0.53	0.78
	Above	0.32	0.33	0.97	929.00	0.331	-0.33	0.98
LV-RD	**Intercept**	0.23	0.50	0.46	929.00	0.648	-0.75	1.21

	Group	-0.33	0.35	-0.95	929.00	0.342	-1.02	0.35
	Age	0.00	0.01	0.00	929.00	0.997	-0.02	0.02
	Gender	-0.36	0.19	-1.90	929.00	0.057	-0.73	0.01
	TSNR	0.02	0.01	1.33	929.00	0.183	-0.01	0.04
	Below	0.25	0.34	0.74	929.00	0.462	-0.42	0.92
	Above	0.40	0.34	1.16	929.00	0.245	-0.27	1.06
LD-RV	**Intercept**	0.55	0.49	1.13	929.00	0.259	-0.41	1.51
	Group	-0.06	0.34	-0.16	929.00	0.869	-0.73	0.62
	Age	-0.02	0.01	-2.24	929.00	0.025*	-0.04	0.00
	Gender	-0.19	0.19	-1.03	929.00	0.305	-0.55	0.17
	TSNR	0.03	0.01	2.42	929.00	0.016*	0.01	0.05
	Below	-0.84	0.33	-2.53	929.00	0.011*	-1.50	-0.19
	Above	0.64	0.33	1.91	929.00	0.057	-0.02	1.29

References

Allen EA, Erhardt EB, Damaraju E, Gruner W, Segall JM, Silva RF, et al. A Baseline for the Multivariate Comparison of Resting-State Networks. Front Syst Neurosci 2011; 5: 1–23.

Asman AJ, Bryan FW, Smith SA, Reich DS, Landman BA. Groupwise multi-atlas segmentation of the spinal cord's internal structure. Med Image Anal 2014; 18: 460–471.

Barry RL, Rogers BP, Conrad BN, Smith SA, Gore JC. Reproducibility of resting state spinal cord networks in healthy volunteers at 7 Tesla. Neuroimage 2016; 133: 31–40.

Baxter LR, Mazziotta JC, Phelps ME, Selin CE, Guze BH, Fairbanks L. Cerebral glucose metabolic rates in normal human females versus normal males. Psychiatry Res 1987; 21: 237–245.

Biswal BB, Mennes M, Zuo X-N, Gohel S, Kelly C, Smith SM, et al. Toward discovery science of human brain function. Proc Natl Acad Sci 2010; 107: 4734–4739.

Calabrese M, Favaretto A, Martini V, Gallo P. Grey matter lesions in MS: from histology to clinical implications. Prion 2013; 7: 20–7.

Cox RW. AFNI: software for analysis and visualization of functional magnetic resonance neuroimages. Comput Biomed Res 1996; 29: 162–173.

Filippi M, Valsasina P, Misci P, Falini A, Comi G, Rocca MA. The organization of intrinsic brain activity differs between genders: A resting-state fMRI study in a large cohort of young healthy subjects. Hum Brain Mapp 2013; 34: 1330–1343.

Glover GH, Li T-Q, Ress D. Image-based method for retrospective correction of physiological motion effects in fMRI: RETROICOR. Magn Reson Med 2000; 44: 162–167.

Gong G, He Y, Evans AC. Brain connectivity: gender makes a difference. Neurosci 2011; 17: 575–591.

De Graaf WL, Zwanenburg JJM, Visser F, Wattjes MP, Pouwels PJW, Geurts JJG, et al. Lesion detection at seven Tesla in multiple sclerosis using magnetisation prepared 3D-FLAIR and 3D-DIR. Eur Radiol 2012; 22: 221–231.

Harrison DM, Roy S, Oh J, Izbudak I, Pham D, Courtney S, et al. Association of Cortical Lesion Burden on 7-T Magnetic Resonance Imaging With Cognition and Disability in Multiple Sclerosis. JAMA Neurol 2015; 72: 1004–12.

Kandel ER, Schwartz JH, Jessell TM, Siegelbaum SA, Hudspeth AJ, Mack S. Principles of Neural Science. 5th ed. McGraw-Hill Companies, Incorporated; 2013.

Kogler L, Müller VI, Seidel E-M, Boubela R, Kalcher K, Moser E, et al. Sex differences in the functional connectivity of the amygdalae in association with cortisol. Neuroimage 2016; 134: 410–423.

De Leener B, Taso M, Cohen-Adad J, Callot V. Segmentation of the human spinal cord. Magn Reson Mater Physics, Biol Med 2016; 29: 125–153.

Liu H, Stufflebeam SM, Sepulcre J, Hedden T, Buckner RL. Evidence from intrinsic activity that asymmetry of the human brain is controlled by multiple factors. Proc Natl Acad Sci 2009; 106: 20499–20503.

Nelson F, Poonawalla a, Hou P, Wolinsky JS, Narayana P a. 3D MPRAGE improves classification of cortical lesions in multiple sclerosis. Mult Scler 2008; 14: 1214–1219.

Prados F, Ashburner J, Blaiotta C, Brosch T, Carballido-Gamio J, Cardoso MJ, et al. Spinal cord grey matter segmentation challenge. Neuroimage 2017; 152: 312–329.

Prados F, Cardoso MJ, Yiannakas MC, Hoy LR, Tebaldi E, Kearney H, et al. Fully automated grey and white matter spinal cord segmentation. Sci Rep 2016; 6: 36151.

Purves D, Augustine G, Fitzpatrick D, Hall W, Lamantia A-S, White L. Neuroscience. 5th ed. Sunderland, MA: Sinauer Associates, Incorporated; 2012.

Sinnecker T, Dörr J, Pfueller CF, Harms L, Ruprecht K, Jarius S, et al. Distinct lesion morphology at 7-T MRI differentiates neuromyelitis optica from multiple sclerosis. Neurology 2012; 79: 708–714.

Smith SM, Jenkinson M, Woolrich MW, Beckmann CF, Behrens TEJ, Johansen-Berg H, et al. Advances in functional and structural MR image analysis and implementation as FSL. Neuroimage 2004; 23: S208–S219.

Summers PE, Brooks JCW. Chapter 4.1 – Spinal Cord fMRI. In: Quantitative MRI of the Spinal Cord. 2014. p. 221–239.

Szalkai B, Varga B, Grolmusz V. Graph theoretical analysis reveals: Women's brains are better connected than

men’s. PLoS One 2015; 10: 1–30.
Tomasi D, Volkow ND. Gender differences in brain functional connectivity density. Hum Brain Mapp 2012; 33: 849–860.
Xu Z, Conrad BN, Baucom RB, Smith SA, Poulose BK, Landman BA. Abdomen and spinal cord segmentation with augmented active shape models. J Med Imaging 2016; 3: 36002.